Understanding Full-Depth Steric Sea Level Change in the Southwest Pacific Basin using Deep Argo

Ratnaksha Lele [1], **Sarah G. Purkey** [1]

[1]Scripps Institution of Oceanography, University of California San Diego, La Jolla, CA

Key Points:

- Nine years of Deep Argo data in the S.W. Pacific reveals continued warming in the abyss while the mid-depths cooled.
- Waters below 4000 m show an accelerated warming trend with a maximum overall warming rate of 4.1 ± 0.31 m^{o}C yr^{-1} at 5000 m.
- Deep ocean steric expansion contributed 1.3 ± 1.6 mm dec^{-1} to total the local sea level.

Corresponding author: Ratnaksha Lele, `rlele@ucsd.edu`

Abstract

Using nine years of full-depth profiles from 55 Deep Argo floats in the Southwest Pacific Basin collected between 2014 and 2023, we find consistent warm anomalies compared to a long-term climatology below 2000 m ranging between 11 ± 2 to 34 ± 2 m^{o}C, most pronounced between 3500 and 5000 m. Over this period, a cooling trend is found between 2000-4000 m and a significant warming trend below 4000 m with a maximum rate of 4.1 ± 0.31 m^{o}C yr^{-1} near 5000 m, with a possible acceleration over the second half of the period. The integrated Steric Sea Level expansion below 2000 m was 7.9 ± 1 mm compared to the climatology with a trend of 1.3 ± 1.6 mm dec^{-1} over the Deep Argo era, contributing significantly to the local sea level budget. We assess the ability to close a full Sea Level Budget, further demonstrating the value of a full-depth Argo array.

Plain Language Summary

Cold, dense waters formed near polar regions in both hemispheres, sink to great depths and fill-up the majority of the world's deep ocean. Compilation of sparse observations of temperature from global ship-based surveys at roughly 10-year intervals worldwide have shown that sequestration of excess atmospheric heat into the deep ocean has caused these waters to warm steadily since the 1990's into the Present. Not only does this warming have implications for changes in large scale ocean circulation, but is also associated with warming-induced sea level rise. Using a new dataset collected between 2014 and 2023 from 55 freely drifting robotic floats (Deep Argo) which gather crucial bimonthly temperature and salinity data between the surface ocean and the ocean floor, we find the greatest warming trend at a depth of 5000 m of 4 ± 0.3 m^{o}C yr^{-1} and an associated sea level rise rate below 2000 m of 1.3 ± 1.6 mm dec^{-1}. Deep Argo data being collected in ocean basins worldwide are crucial in providing high resolution data of the warming deep ocean and its implications on global sea level, ocean mixing and large-scale ocean circulation.

1 Introduction

The Earth's energy is currently out of balance, with the climate system accumulating 0.5-1 W m^{-2} over the 21st century (Hansen et al., 2011; Von Schuckmann et al., 2016; von Schuckmann et al., 2022; Trenberth et al., 2014; Llovel et al., 2014). One of the most direct and well-documented consequences of this energy imbalance is the rise of global mean surface temperatures and warming in the lower atmosphere (Hansen et al., 2011; Meyer et al, 2014; Steiner et al., 2020). Although these global mean surface temperatures and atmospheric warming effects are most perceptible, they account for only a small fraction of the Earth's energy budget. The oceans accumulate roughly 90% of the excess warming and therefore play a dominant role in sequestering the excess heat and mediating the worst effects of rapid atmospheric warming (Domingues et al., 2008; Levitus et al., 2000, 2005, 2012; Meyer et al, 2014; Cheng et al., 2017; von Schuckmann et al., 2022). One consequence of the increase in ocean heat content is the rise in global mean sea level owing to the thermal expansion, accounting for roughly half the observed sea level rise over the last century (Von Schuckmann et al., 2016). Satellite altimetric estimates the global mean sea level has risen at a mean rate of 3.3 ± 0.4 mm yr^{-1} since the early 1990s (Watson et al., 2015; Dieng et al., 2015; Chambers et al., 2017; Nerem et al., 2018; Ablain et al., 2015; WCRP Global Sea Level Budget Group, 2018).

While the upper ocean (< 2000m) accounts for the majority of accumulated ocean heat content (OHC) over the past 50 years, the deep (below 2000m) and abyssal (below 4000m) oceans have also warmed, contributing roughly 10 % to total ocean heat content changes (Purkey & Johnson, 2010a; Von Schuckmann et al., 2016; von Schuckmann et al., 2022). The deep warming is possibly linked to a decline in Antarctic Bottom Wa-

ter (AABW) formation rates around Antarctica, as well as decadal variability in rate and properties of North Atlantic Deep Water (NADW) (Purkey & Johnson, 2010a, 2012, 2013; Smeed et al., 2014). Furthermore, models suggest the deep and abyssal ocean warming could be an indication of a large scale climatic shift in the overturning circulation (Li et al., 2023; Gunn et al., 2023; Ditlevsen & Ditlevsen, 2023).

Although satellite altimetry can monitor the total rate of sea level rise, it is necessary to understand the components and mechanisms leading to global mean sea level rise and its variability to better predict future sea level rise, as well as understand and quantify any errors in the observations (Llovel et al., 2023; Chen et al., 2020; Barnoud et al., 2021; Chen et al., 2022). Crucially, density-driven volumetric variation (steric variation) from changes in temperature and salinity changes (thermosteric and halosteric respectively) in the ocean is a significant contributor to sea level rise and the global sea level budget (Bindoff et al., 2007; Levitus et al., 2012; WCRP Global Sea Level Budget Group, 2018; Llovel et al., 2019). *In-situ* hydrographic measurements sampling the ocean sub-surface are vital to measuring the steric component of sea level rise. For most of the 20th century, sampling of oceanographic properties was sporadic, with low spatial and temporal coverage. In the early 2000s, Argo (also referred to as core-Argo) revolutionized our ability to monitor steric variability in the upper 2000 m, maintaining a fleet of roughly 4000 floats worldwide, allowing for accurate monitoring of temperature and salinity changes on high temporal (1 month) and spatial (1 deg x 1 deg) resolution around the globe (Roemmich et al., 2019).

Despite these advances in global ocean observational capabilities in the last few decades, the deep ocean below 2000 m remains vastly undersampled in comparison. Most ocean observations including measurements from the core-Argo fleet are limited to the top 2000 m (Abraham et al., 2013), limiting our understanding of steric changes occurring in the deep ocean. Deep steric estimates rely on decadal observational programs such as the World Ocean Circulation Experiment and the Global Ocean Ship-based Hydrographic Investigations Program (GO-SHIP) (Talley et al., 2016; Gould et al., 2004; Roemmich et al., 2012; Riser et al., 2016). These hydrographic measurements have shown an increase in deep ocean temperatures in most deep ocean basins below 4000 m, contributing to sea level rise estimates at a rate of approximately 1mm dec $^{-1}$ (Purkey & Johnson, 2010a; Purkey et al., 2014; Desbruyères et al., 2016; Purkey et al., 2019), roughly 10-15% of total steric sea level rise (Von Schuckmann et al., 2016; von Schuckmann et al., 2022; Llovel et al., 2019).

The implementation of a 1250-float Deep Argo Array aims to alleviate obstacles of data-gathering in the deep and abyssal ocean (Johnson et al., 2015; Roemmich et al., 2019). The floats capable of measuring down to 4000 m or 6000 m depending on the model specifications, can potentially reduce deep steric uncertainty to a fifth of current estimates from using only hydrographic data. Pilot arrays of Deep Argo floats have been deployed since early 2014 in deep basins around the globe. Initial data at bi-monthly resolution from pilot Deep Argo arrays deployed in the Southwest Pacific, Argentine and Brazil basins have already shown continued warming in the deepest parts of the basin below 4000 m and have provided warming rates in the AABW layers with a high degree of accuracy (Johnson et al., 2019, 2020; Johnson, 2022).

In this study, we extend the analysis of Johnson et al., 2019 by incorporating temperature and salinity data below 2000 m from 4954 full-depth profiles taken by 55 Deep Argo floats in the Southwest Pacific (SWP) Basin between July 2014 and May 2023 to evaluate the continued deep warming trends in the basin. Further, we expand on this analysis to estimate the trend and variability in the deep (>2000 m) steric component of the local sea level budget, to better assess its closure in the SWP Basin. Data and methodology used to analyze data from a core Argo climatology, Deep Argo float data, and satellite-gridded products of sea surface height and ocean mass are described in Section 2. We present the main results in Section 3, followed by a discussion surrounding the results

114 in Section 4. These results highlight the consequences of the deep ocean warming and
115 steric sea level rise and demonstrates the value of making high quality, high resolution
116 measurements of the deep ocean.

2 Data and Methods

2.1 Deep Steric Contributions using Deep Argo

119 In the SWP Basin between 10^oS and 50^oS and 170E^o and 130^oW, we consider pro-
120 files collected by 55 Deep Argo floats between July 2014 and May 2023 (Figure 1, yel-
121 low lines). Only profiles that reach the maximum float depth (6000 m) or the sea floor
122 are considered in this study. A total of 4954 profiles collected from the 55 floats are used
123 for the analysis, of which 85% reached at least 5000m (Supporting Information Figure
124 1, purple). All floats carried a SeaBird Scientific SBE-61 CTD (Conductivity-Temperature-
125 Depth) sensor with an accuracy of 0.002psu, $1m^o$ C and 2dbar, respectively. Only down-
126 cast profiles were considered and only data with good quality flag data are used.

127 The WOCE hydrographic climatology (Gouretski & Koltermann, 2004) represents
128 the averaged properties in the basin over the 1980-2004 time period, using data from hy-
129 drographic observations objectively mapped onto a $1^o \times 1^o$ spatial grid. The deep ocean
130 data considered here below 2000 m consist of 15 depth levels from 2000 m to a maximum
131 of 5750 m, with a depth-spacing of 250 m.

132 The salinity, temperature and pressure profile data are used to calculate absolute
133 salinity, conservative temperature Θ and depth using TEOS-10 equation of state (Feistel,
134 2012; McDougall, 2011). The WOCE climatology is linearly interpolated at the location
135 of each Deep Argo profile in latitude, longitude and depth coordinates. The Θ and ab-
136 solute salinity anomalies are then calculated as the difference between Deep Argo and
137 WOCE estimates at each profile location (e.g. Figure 2, 3a).

138 A linear trend in Θ over the nine year Deep Argo period is calculated using a least
139 squares fitting procedure following (Wunsch, 1996; Johnson et al., 2019) at each verti-
140 cal WOCE level (e.g. Supporting Information Figure S2, Table S1). In addition the full
141 time period, the linear trend from January 2016 to December 2019 and January 2020
142 through May 2023 are also calculated (e.g. Figure 3b). Degrees of freedom for comput-
143 ing confidence limits on Θ anomalies and trends at each vertical level are calculated by
144 assuming statistical independence between profile data from each float. However, a tem-
145 poral decorrelation time scale of 60 days is considered for profiles from the same float
146 to be considered independent for the deep ocean (Johnson et al., 2015, 2019), such that,
147 if there a total N_{60} profiles within a 60-day period, each profile contributes $1/N_{60}$ de-
148 grees of freedom within that time frame. The effective degrees of freedom generally de-
149 crease with an increase in depth and vary between 850-750 between 2000 m and 5000
150 m, a factor of $\sim$6 reduction, whereas at 5500 m the effective degrees of freedom, reduce
151 by a factor of $\sim$4 to around 200 (Supporting Information, Figure S1). We computed 5%–95%
152 confidence intervals (two-tailed 90%) using the standard deviations (σ) and the effec-
153 tive degrees of freedom estimated above assuming Student's t-distribution and use the
154 same significance tests to assess confidence intervals throughout the rest of the study.
155 The reduction in degrees of freedom has negligible (<1%) effect on the estimated con-
156 fidence interval as the Student t-distribution score asymptotes to $\sim$2 for such large val-
157 ues of degrees of freedom.

158 The Argo profiles were also used to examine the temporal variability of the inte-
159 grated steric sea-level. First density anomalies were calculate at each vertical level with
160 respect to the WOCE climatology as described in the methods used for Θ anomalies de-
161 scribed above. Then, following (Gill & Niller, 1973) and (Tomczak & Godfrey, 1994),

the steric sea-level anomaly η_s can be computed as:

$$\eta_s = -\frac{1}{\rho_0} \int_{z_2}^{z_1} \rho'$$

(1)

where ρ_0 (~ 1028 kg m^{-3}) is a reference density and ρ' is the local density anomaly calculated using the Thermodynamic Equation of Seawater (TEOS-10, (McDougall, 2011) equation of state. The expression is vertically integrated from the maximum local depth z_2 to the top interface (z_1, here 2000 m) to obtain the integrated sea-level anomaly at the location.

After the steric anomalies with respect to the climatology are calculated at each vertical level (Figure 2d), the anomalies are integrated between the bottom and the top (2000 m) to calculate the total steric contribution at each location (e.g. Figure 3c), hereafter referred to as "deep steric" anomalies. Since the bottom reference for integrating steric anomalies z_2 varies with changes in the bottom depth as the float traverses the basin, the total steric anomaly calculated from Equation 1 represents the deep steric contribution below 2000 m at each float location.

A least squares fitting is used to estimate the trend in the integrated steric height between the bottom and 2000 m (Figure 3d) . The significance estimate on the trend is calculated similarly as for the trend in Θ using a Student t-distribution and effective degrees of freedom using a 60-day decorrelation timescale (Figure 3d). To show the relative contribution of the deep steric signal at various depth levels, we also repeat this procedure by only calculating steric height anomalies integrated to 3000 m, 4000 m, and 5000 m as well (Equation 1 : $z_2 = \{2000, 3000, 4000, 5000 \}$, Figure 3c).

2.2 A Local Sea Level Budget using Deep Argo

Here we select a single $5^o \times 5^o$ box between between 30-35°S and 170-165°W in the SWP Basin with over 6 years of continuous monthly deep argo data to examine the local sea level budget (Figure 1b, green box) and test closure of the local sea level budget.

The Mean Sea Level change (MSL) within the study region can be expressed as a function of time (t) as :

$$MSL(t) = MSL_{\text{mass}}(t) + MSL_{\text{steric}_{(0-2000)}}(t) + MSL_{\text{steric}_{(2000-btm)}}(t)$$

(2)

where $MSL_{\text{steric}_{(0-2000)}}(t)$ represents the steric contribution of the ocean due to density-driven volumetric changes in the upper 2000 m in the mean sea level, $MSL_{\text{mass}}(t)$ reflects the mass anomaly in the region either due to the movement of water into and out of the region or addition to the ocean mass of the region and $MSL_{\text{steric}_{(2000-btm)}}(t)$ is the steric contribution below 2000 m, hereafter the "deep steric" signal.

The left-hand side of Equation 2 can be retrieved through satellite altimetry. We use monthly gridded sea level anomaly observations from AVISO (AVISO website https://www.aviso.altimetry.fr/en/data/products/) to estimate $MSL(t)$ in the basin (Supporting Information Figure S3, top). The gridded sea surface height product consists of sea surface anomalies computed with respect to a 20-year reference period (1993-2012). GIA effects are corrected for using the ICE6G-D model (Peltier et al., 2018). Once geophysical and instrument corrections have been applied, altimetric sea surface height measurements are generally accurate to within 1 cm (Stammer & Cazenave, 2017; WCRP Global Sea Level Budget Group, 2018).

The time series of variation of local ocean mass anomaly in the study region, $MSL_{\text{mass}}(t)$, is estimated using NASA's GRACE and GRACE-Follow On data (GRACE from hereon)

(Tapley et al., 2004) derived from the Jet Propulsion Laboratory (JPL) RL06M spherical mass concentration block "mascon" solutions (Watkins et al., 2015). The mascon solutions have shown improvements over spherical harmonic solutions established in the first decade of GRACE observations. The JPL RL06M uses a-priori constraints in space and time to estimate global, monthly gravity fields in terms of equal-area $3^o \times 3^o$ spherical cap mass concentration functions to minimize the effect of measurement errors resulting improved signal-to-noise (S/N) ratios (Watkins et al., 2015; Tapley et al., 2019). Data from other mascon solutions (e.g. Center for Space, GeoforschungsZentrum) are within the margin of error for this $5^o \times 5^o$ region and are therefore not used comparatively (e.g. Llovel et al., 2019; Chen et al., 2020). We use the JPL mascon solution in the SWP Basin to estimate $MSL_{\mathrm{mass}}(t)$ in Equation 2 (Supporting Information Figure S3, bottom). The GRACE data have the largest footprint amongst the gridded data products used here. Although the mapped product available is of a higher resolution of $0.5^o \times 0.5^o$, the $3^o \times 3^o$ mascon approximately matches the accuracy and native resolution of the GRACE satellites (Wiese et al., 2016).

The upper ocean steric height, $MSL_{\mathrm{steric}(0-2000)}(t)$, is estimated using the Argo Climatology (Roemmich & Gilson, 2009) which consists of temperature and salinity data from thousands of core-Argo float profiles, objectively mapped onto a $0.5^o \times 0.5^o$ grid worldwide. We use temperature and salinity data from the climatology in the basin to estimate the upper ocean steric contribution above 2000 m using Equation 1 (Supporting Information Figure S3, middle). We only consider the Roemmich and Gilson (2009) climatology as the dataset incorporates delayed-mode quality control data, alleviating pitfalls of biased salinity measurements from instrument calibration drift noted recently (Wong et al., 2023).

Finally, within this $5^o \times 5^o$ region, profile data collected by three Deep Argo Floats (WMO ID: 5902444, 5902528, 5905760) between Spring 2016 and January 2023 is used to calculate monthly-averaged deep steric anomalies. The deep steric anomalies computed using the floats $MSL_{\mathrm{steric}(2000-btm)}(t)$ can be combined with the upper ocean steric anomalies from Argo climatology $MSL_{\mathrm{steric}(0-2000)}(t)$, to compute the full-depth steric anomaly time series between 2016 and 2023 (Supporting Information Figure S4, purple post-2016). For this local $5^o \times 5^o$ region in the SWP basin, we do not include additional terms associated with mass redistribution from gravitational, rotation and deformation (GRD) effects resulting from water mass exchange between the land and ocean from the hydrological cycle and cryospheric input (Frederikse et al., 2020; Moreira et al., 2021; Harvey et al., 2021), or from ocean bottom deformation (OBD) effects (Frederikse et al., 2017; Vishwakarma et al., 2020).

At sub-yearly and inter-monthly time scales the amplitude and phase agreement between in the time series of the budget terms in this is $5^o \times 5^o$ region large and could be due to a variety of factors including different footprints of the satellite data in space and in time, artifacts of various interpolation and mapping schemes used to create the gridded products among others. Therefore, to access budget closure and extricate seasonal variability and associated amplitude mismatch in the time series, the mean, annual and semi-annual cycle is removed from the monthly time series of each term in Equation 2 (Supporting Information Figure S5), leaving only the trend and variability associated with higher-order harmonics in the signal (Bendat and Piersol (1986), Figure 4). Results and discussion in Sections 3 and 4 only include data with this modified time series.

Here, we only focus on this example $5^o \times 5^o$ region because it is best suited for the full sea level budget calculation as it is the deepest region in the basin with an average depth of roughly 5000 m, enabling optimal evaluation of the deep steric component in the budget. Further, by choosing this region, we maximize the length of contemporaneous data from multiple floats (over 6 years from three separate floats), as well as avoid regions near coastal boundaries and large bathymetric features (e.g. Tonga-Kermadec

Trench in the SWP Basin) associated with signal leakage errors in the GRACE data (Wiese et al., 2016; Watkins et al., 2015) with the potential to bias results of the budget. The deep steric anomalies computed using the floats $MSL_{\text{steric}(2000-btm)}(t)$ can be combined with the upper ocean steric anomalies from Argo climatology $MSL_{\text{steric}(0-2000)}(t)$, to compute the full-depth steric anomaly time series between 2016 and 2023 (Supporting Information Figure S4, purple past 2016). If the Deep Argo program is continued and reaches global implementation, a similar analysis will be possible globally, for purposes of computing global averages of the deep steric signal.

3 Results

3.1 Θ and Steric Anomaly and Trends in the Basin

Using 4954 profiles from 55 Deep Argo floats between July 2014 and May 2023 within the SWP basin we calculate changes in Θ compared to a long-term WOCE hydrographic climatology (Gouretski & Koltermann, 2004) (1980-2004, mean 1995). We find statistically significant warming in the deepest portions of the basin, consistent with findings from previous studies which use both hydrographic and float data (Purkey & Johnson, 2010a; Kouketsu et al., 2011; Johnson & Lyman, 2020). The Θ anomaly reveals that the entire depth range between 2000 m and bottom is warmer than the climatological era of roughly two to three decades prior. The warming is most pronounced between 3800 m and 4200 m with Θ anomalies in excess of 30±2.8 m ^{o}C. The warming in the deepest layer at 5750 m is roughly between 12±4 m ^{o}C (Figure 3a). The uncertainties are largest near the bottom, where the effective degrees of freedom are smaller due to fewer total profiles in that depth range (Supporting Information Figure S1), as well as between 2000 m - 3000 m, which corresponds to an increase in vertical temperature gradient associated with the transition between NADW and other mode and intermediate waters (Talley et al., 2007).

The warming trend between 2014 and 2023 from the Deep Argo floats is positive and statistically significant below 4000 m in the basin. The average warming below 4000 m is 2.2 ±0.25 m m^{o}C yr^{-1} with the highest rate of temperature increase found near 5000 m of 4.1±0.31 m m^{o}C yr^{-1} (Figure 4b, Supporting Information Figure S2). Between 5000 m and the bottom the rate of increase in Θ is roughly 3.1 ±0.3 m m^{o}C yr^{-1} and is consistent with previous studies which have found similar rate of warming in the abyssal AABW layers of the SWP Basin (Purkey & Johnson, 2010a; Purkey et al., 2019; Johnson et al., 2019). Although the layers shallower than 4000 m have warmed on average 21 ±3 ^{o}C compared to the WOCE climatology period (Figure 3a), a cooling trend has been observed by the floats in the 9 year period of -1.2 ±0.28 m m^{o}C yr^{-1} between 4000 m and 2000 m, with a maximum cooling trend near 2500 m of -1.96 ±0.46 m m^{o}C yr^{-1} (Figure 3b, Supporting Information Figure S2, Table S1). The accelerated warming in the deep and abyssal waters below 4000 m is associated with isotherm heaving and the shrinking in the volume of the AABW layer and homogenization of temperature and density gradients for much of the basin westward of the East Pacific Rise (EPR) ($\sim 130^{o}$W) (Purkey & Johnson, 2010b; Lele et al., 2021).

Examination of the shorter term trends show some internal variability in the warming rates, indicating the mid-depth cooling and deep water may be accelerated in the last three years of the time series. The first two years of the time series (2014-2015) have the most sparse coverage and thus are not considered for the shorter time period trends (Figure 3b, e). The four year trend from 2016 to 2019 shows pronounced cooling (-4.27 ±1.3 m^{o}C yr^{-1}) between 3225 m and 4000m compared to the full 9 year time series (-0.72 ±0.49 m^{o}C yr^{-1}) and stronger warming below 4500m in the second half of the time series.

We calculate the total steric anomaly integrated between 2000 m and the bottom for all 4954 profiles and find the average deep steric expansion of 7.9 ± 1 mm compared

to the climatology. The float data indicate that the trend in deep steric contribution to the local sea level rise budget integrated between 2000 m and 6000 m is 0.13 ± 0.16 mm yr^{-1} (1.3 ± 1.6 mm dec^{-1}), partitioned as a steric contraction of -0.38 ± 0.04 mm yr^{-1} between 2000 m and 4000 m and, a steric expansion of 0.52 ± 0.16 mm yr^{-1} between 4000 m and 6000 m (Figure 3c, d). The deep steric trends in the SWP basin are robust and statistically significant over the 9 year period considered here. We also find agreement between our estimates and previous estimates in the basin using decadal hydrographic surveys (Purkey & Johnson, 2010a), in addition to global mean residual estimates computed using residuals combining satellite altimetry and gravimetry (Llovel et al., 2019; WCRP Global Sea Level Budget Group, 2018; Horwath et al., 2022).

3.2 Sea Level Budget Closure in a local $5^o \times 5^o$ Region

The local sea level budget over the $5^o \times 5^o$ region between 30^oS and 35° and 170^oW and 165^oW showed general closure within 1-σ uncertainty estimates (Figure 4b, shading) with an improved agreement when the Deep Argo data is included. The deep steric anomaly amplitude (below 2000 m) is roughly 10% of amplitude variation shown by the upper ocean steric anomaly (Figure 4a, teal), consistent with previous studies (Purkey & Johnson, 2010a; Chambers et al., 2017; Llovel et al., 2019). The average deep steric contribution was 7.2 mm over the 6 years period of monthly Deep Argo data, which added to the total steric anomaly between 2016 and 2023 (Supporting Information Figure S4, purple). This average estimate of deep steric contribution calculated from the three floats in the $5^o \times 5^o$ region are within the our overall estimates of the average deep steric contribution for the SWP basin below 2000 m of 7.9 ± 1 mm (Section 3.1, Figure 3d).

The residual between SSH anomaly and the Steric signals (SSH - Full Steric and SSH - Upper Steric Argo; "SSH residual" hereafter) are compared against satellite-derived GRACE mass anomaly estimates (Figure 4b, purple and gray). The mean absolute difference of the time series between full SSH residual (including Deep Argo data) and GRACE is 2.6 ± 0.25 mm in the period between 2016 and 2022 (Figure 4b), excluding the the period between June 2017-June 2018 between the GRACE and GRACE-Follow On mission which render no data, as seen in the GRACE time series (Supporting Information Figure S5).

The residual estimates which incorporate deep steric anomaly data from Deep Argo (SLA - Deep Argo, Figure 4b, purple) explains roughly 7% more variance in the underlying GRACE signal than the residual without this estimate (Figure 4b, gray). While the increase in explained variance and consequently the mean squared error is comparatively modest, we note the small spatial scale of this sea level budget analysis in a $5^o \times 5^o$ region of the basin. Incorporating more float data over a larger spatial scale as well as averaging out satellite SSH and gravimetric signals from a larger swath of the SWP, could yield better agreements between the residual time series and GRACE signal.

4 Discussion and Conclusions

Using Deep Argo float data in the SWP basin from the past 9 years we find that the AABW layer in the basin has warmed on average between 12 ± 4 m ^{o}C (Figure 2a) compared to the WOCE-era leading to the disappearance of the coldest isotherms and reducing stratification in abyssal parts of the basin, consistent with other studies that have relied on decadal hydrographic observations (Purkey & Johnson, 2010a; Lele et al., 2021). The data also show substantial warming at mid-depths between 2000 m - 4000 m with a peak warming 30 ± 2.8 m ^{o}C (Figure 2a). The availability of nearly a decade of full-depth bi-monthly observations spanning the basin with over 4954 profiles prove valuable in reducing statistical uncertainty, which can often plague the determination of statistical significance in results from decadal hydrographic observations.

The rate of warming implied by our results is also consistent with the idea of accelerated warming in the deepest portions of the basin. Hydrographic data collected between the 1990s and 2000s found the warming rate to be roughly 1 m^{o}C yr^{-1} (Purkey & Johnson, 2010a) in the basin, which had accelerated to 2 m^{o}C yr^{-1} in the subsequent decade between 2000s and 2010s (Purkey et al., 2019). A similar study conducted using Deep Argo within the basin through 2019 found warming rates between 3±1 m^{o}C yr^{-1} in the bottom water regime below 5000 m (Johnson et al., 2019). Here, using a full 9-years of data, we find the warming trend slightly higher than (Johnson et al., 2019) below 5000 m of 3.1 ±0.3 m^{o}C yr^{-1}, and show the trend between 2020-2023 is larger than 2016-2019 (Figure 3b). Furthermore, this study shows the mid-depth cooling might also be accelerating (Figure 3b).

We note that using a decadal climatology such as WOCE which uses sparse hydrographical data from ship-based surveys, mapped into an optimally interpolated product can introduce additional uncertainty and bias in the results. Regions in the basin such as the EPR and the abyssal plains west of the Rise with multiple different repeat hydrographic lines passing through them (e.g. P06, P15 and P16 and P31), could have much less uncertainty and better signal-to-noise ratios than large swaths of regions with only one or two decadal full-depth observations. However, temperature anomalies and trends calculated from thousands of profiles over almost a decade, as well as agreement with past estimates in the basin, lend substantial credence to the results presented in this study. Once Deep Argo has been implemented long enough, local trends can be calculated directly eliminating the need for a climatology.

We use the simultaneous temperature and salinity measurements by all the 55 floats in the basin to compute density anomalies and steric anomalies compared to the WOCE climatological data, at each each vertical level between 2000 m and 5750 m or the bottom using Equation 1 (e.g. Figure 3d). Our estimate of deep steric sea level rise of 1.3 ± 1.6 mm dec^{-1} is robust and falls within previous estimates in the basin conducted using hydrography, as well as other global estimates using residual sea level rise budget calculations (Purkey & Johnson, 2010a; Purkey et al., 2019; Llovel et al., 2019). We also demonstrate a slight improvement in the overall closure of a local sea level budget estimated within a $5^o \times 5^o$ region of the basin when using the full-depth steric height anomalies computed using Deep Argo data versus using core-Argo steric height anomalies in the upper 2000m. When the vision of a global Deep Argo array is realized, the data will prove invaluable in providing insights into the changing abyssal oceans, better inform climate models, constrain model-based reanalysis products of past deep ocean change and improve future projections of sea level rise.
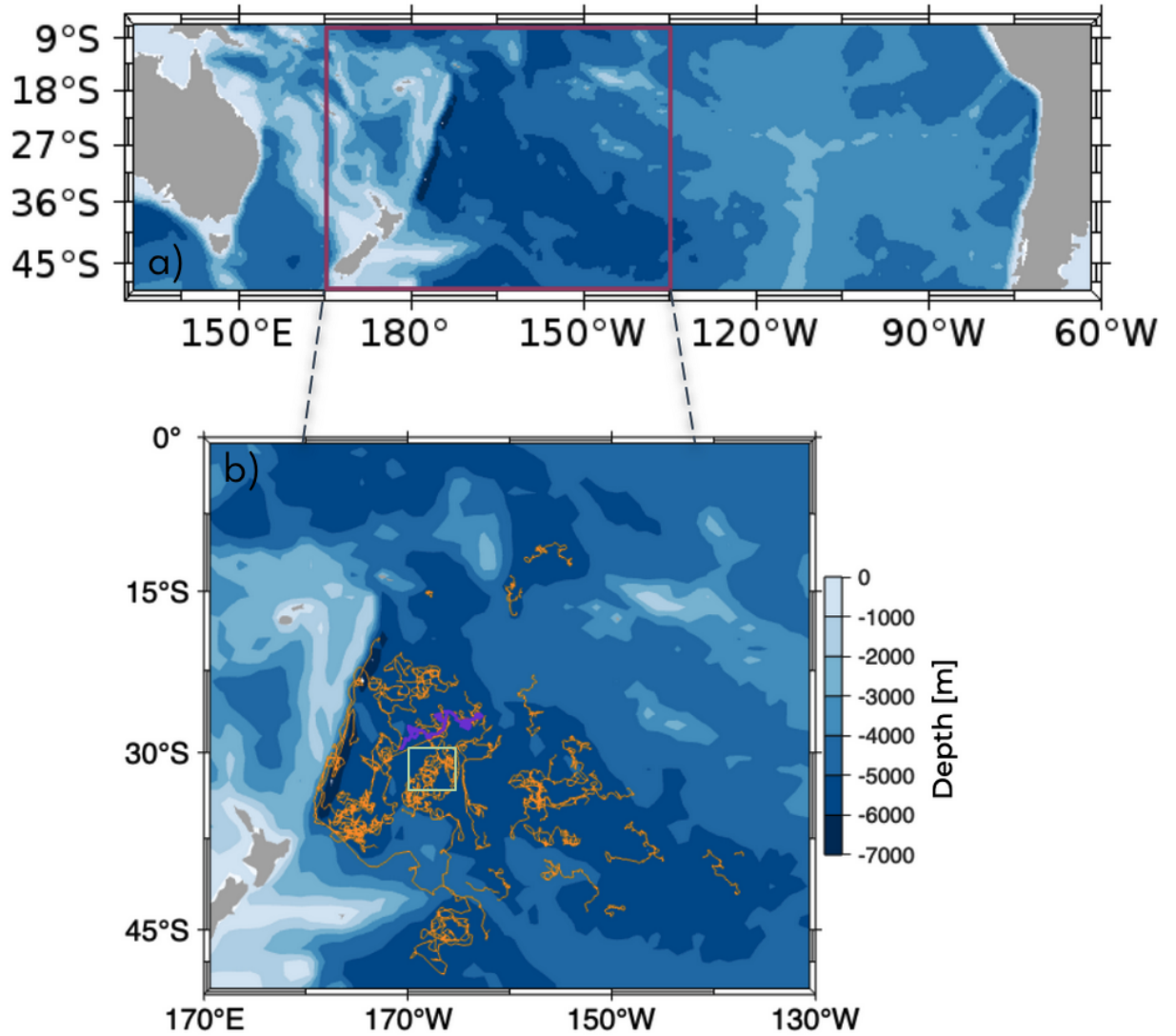
Figure 1. (a) Map of the South Pacifc with the SWP Basin highlighted (purple), b) The location of 55 Deep Argo floats in the SWP Basin used in the study. Purple marks the location of float profiles shown in Figure 2 and 3 and, the green 5° x 5° box between 30-35°S and 170-165°W shows trajectories from three floats used for the sea level budget calculation discussed in Section 2.2.
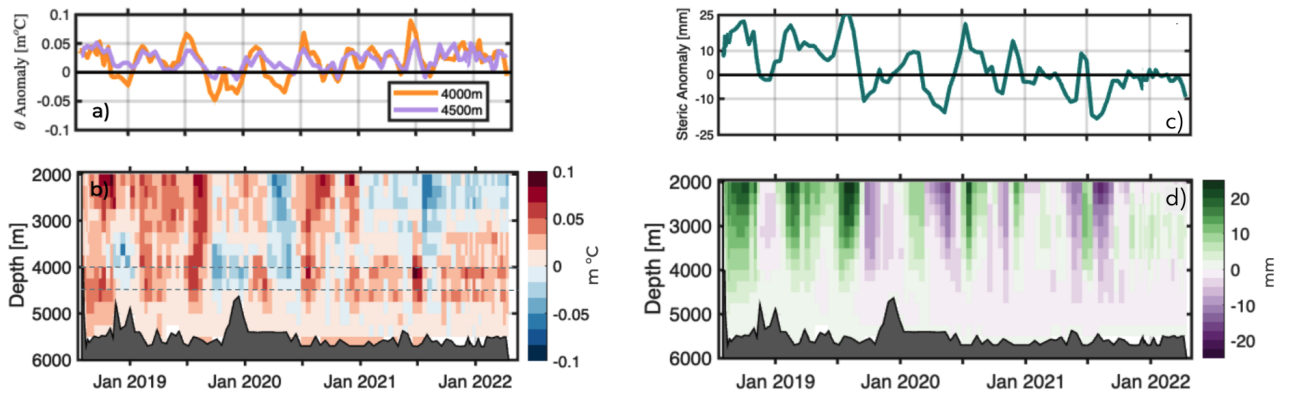
Figure 2. a) Conservative Temperature (Θ) anomaly time series at 4000 m and 4500 m computed with respect to the WOCE hydrographic climatology along the Deep Argo float trajectory (Figure 1, purple), b) Θ anomalies along the float trajectory between 2000 m and the bottom, also computed referenced to the WOCE climatology. c) Steric Anomaly(2000 m-5750 m) time series and, d) Steric Anomaly along one Deep Argo float referenced to the WOCE climatology along the float trajectory. Locations of time series in panel a) and c) marked by the horizontal dashed line. The float trajectory in the basin is shown in Figure 1 (purple).
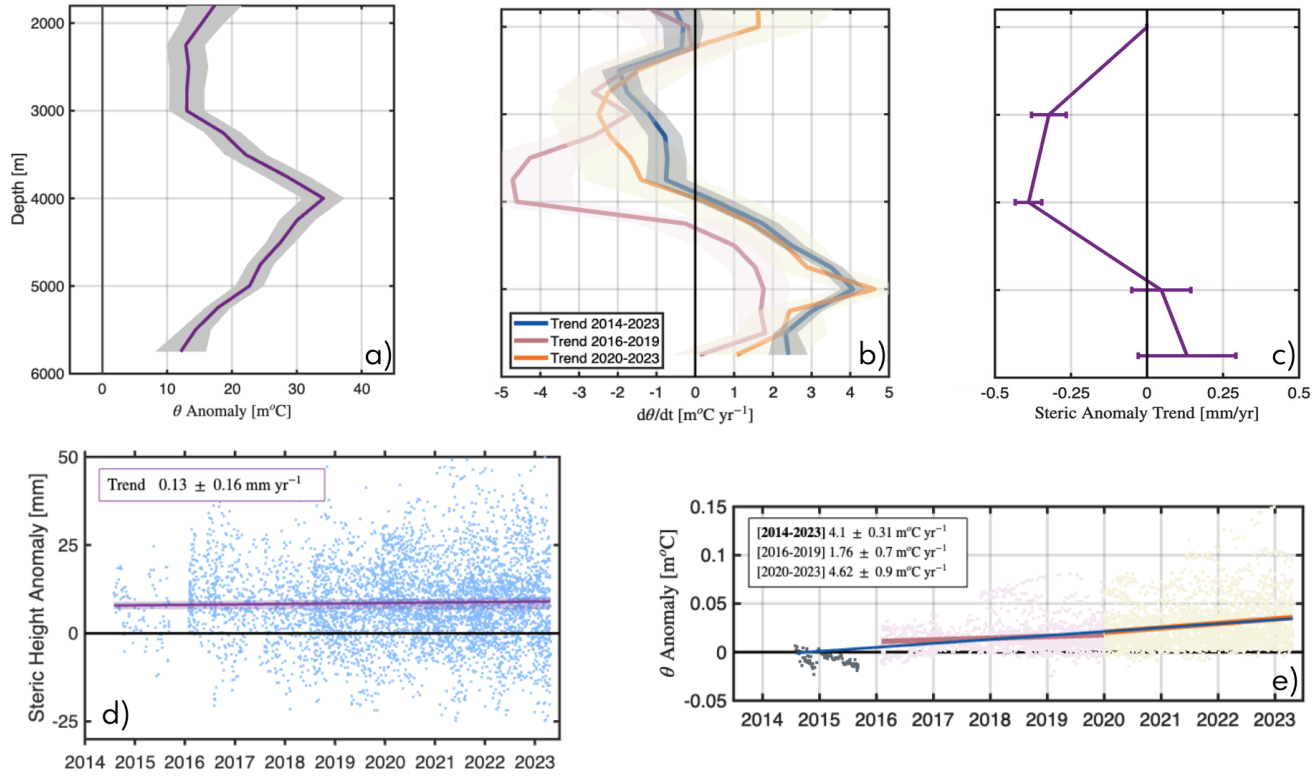
Figure 3. a) Conservative temperature Θ anomaly computed using all Deep Argo profiles in the basin with 95% confidence intervals (grey shading). b) Θ anomaly trend vs Depth [m^{o}C yr^{-1}] computed using all available float data in the basin considering the full time period of Deep Argo data (2014-2023, blue), an early time period (2016-2019, pink), and a later time period (2020-2023, orange), c) Deep Steric Anomaly trend [mm/yr] between depth-levels (m) and 2000 m, computed as using the depth integral between depth-levels (3000m, 4000 m , 5000 m , 5750 m) and 2000 m respectively using Equation 1,d) Trend in deep steric anomalies [mm yr $^{-1}$] between 2000 m and 5750 m computed from data from all Deep Argo profiles used in the study. Trend and 95% confidence interval shown is the same as in Figure 3c (5750 m), e) Θ anomaly trend [m^{o}C yr^{-1}] showing an accelerated warming trend at 5000 m showing trends between 2016-2019 (pink), 2020-2023 (yellow) and the 2014-2023 (blue). The trends computed here are same in panel b (5000 m).
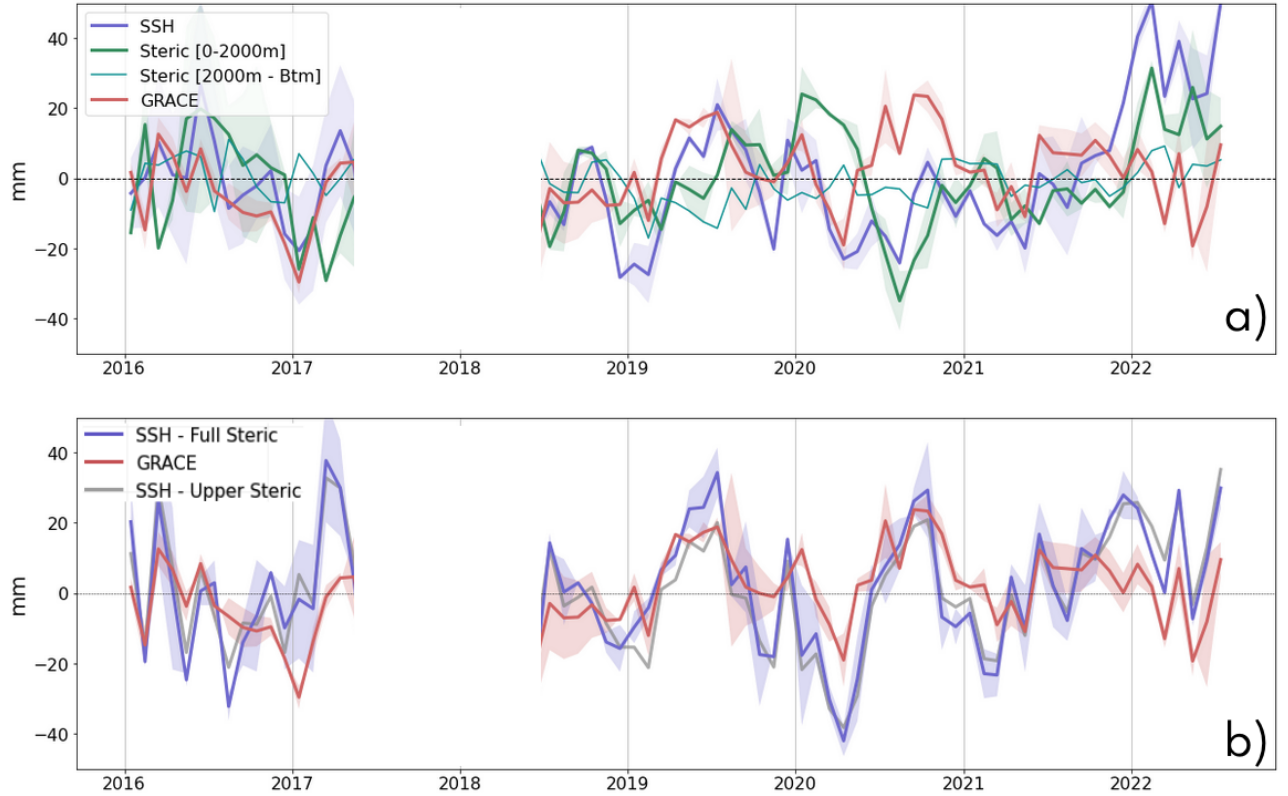
Figure 4. a) Times series of the components in the sea level budget considered in the study in the 5x5 degree region of the SWP Basin described in Section 2.2, i.e. Sea Surface Height anomalies (SSH) [purple], upper ocean steric height anomalies using the Argo Climatology [green], deep ocean steric height anomalies composited using 3 Deep Argo floats in the region [teal], GRACE-derived gravimetric mass anomalies [red]. b) Residual mass anomalies computed as the difference between SSH anomaly and the full-depth (surface to bottom) steric anomaly [purple], compared to satellite-derived gravimetric mass anomalies from GRACE [red]. Residual mass anomalies computed between SSH anomaly and upper-ocean [0-2000 m] steric from the Argo Climatology is shown for comparison (gray). To consider the contribution of the deep steric estimates made using Deep Argo to the budget, we only consider the time period beyond 2016 marking the beginning of the float deployment in this 5x5 region. The mean, annual and semi-annual harmonics have been removed from all time series. Shading denotes 1-σ uncertainty for the respective estimates. Note that the period between mid-2017 and mid-2018 marking the gap in GRACE data has been masked and is not used for calculation presented here.

Acknowledgments

Open Research

All data used in this study is public. The Argo data were downloaded from the Argo Global Data Assembly Center (Argo, 2000). GRACE/GRACE-FO Mascon data are available from NASA/JPL (2023). The sea level anomaly product can be downloaded from Copernicus Climate Change Service (2018).

References

Ablain, M., Cazenave, A., Larnicol, G., Balmaseda, M., Cipollini, P., Faugère, Y., ... Benveniste, J. (2015). *Improved sea level record over the satellite altimetry era (1993-2010) from the Climate Change Initiative project.* doi: 10.5194/os-11-67-2015

Abraham, J., Baringer, M., Bindoff, N., Boyer, T., Cheng, L., Church, J., ... others (2013). A review of global ocean temperature observations: Implications for ocean heat content estimates and climate change. *Reviews of Geophysics*, *51*(3), 450–483.

Argo. (2000). Argo float data and metadata from Global Data Assembly Centre (Argo GDAC). *Seanoe*. doi: http://doi.org/10.17882/42182

Barnoud, A., Pfeffer, J., Guérou, A., Frery, M. L., Siméon, M., Cazenave, A., ... Ablain, M. (2021). Contributions of Altimetry and Argo to Non-Closure of the Global Mean Sea Level Budget Since 2016. *Geophysical Research Letters*, *48*(14). doi: 10.1029/2021GL092824

Bendat, J. S., & Piersol, A. G. (1986). *Random data: Analysis and measurement procedures* (2nd ed.). New York: J. Wiley.

Bindoff, N. L., Willebrand, J., Artale, V., A, C., Gregory, J., Gulev, S., ... Unnikrishnan, A. (2007). Climate Change 2007: The Physical Science Basis. Contribution of Working Group I to the Fourth Assessment Report of the Intergovernmental Panel on Climate Change. In S. Solomon et al. (Eds.), (chap. Observations: Oceanic Climate Change and Sea Level.). New York: Cambridge University Press.

Chambers, D. P., Cazenave, A., Champollion, N., Dieng, H., Llovel, W., Forsberg, R., ... Wada, Y. (2017). *Evaluation of the Global Mean Sea Level Budget between 1993 and 2014.* doi: 10.1007/s10712-016-9381-3

Chen, J., Cazenave, A., Dahle, C., Llovel, W., Panet, I., Pfeffer, J., & Moreira, L. (2022). *Applications and Challenges of GRACE and GRACE Follow-On Satellite Gravimetry.* doi: 10.1007/s10712-021-09685-x

Chen, J., Tapley, B., Wilson, C., Cazenave, A., Seo, K. W., & Kim, J. S. (2020). Global Ocean Mass Change From GRACE and GRACE Follow-On and Altimeter and Argo Measurements. *Geophysical Research Letters*, *47*(22), 1–9. doi: 10.1029/2020GL090656

Cheng, L., Trenberth, K. E., Fasullo, J., Boyer, T., Abraham, J. P., & Zhu, J. (2017). *Improved estimates of ocean heat content from 1960 to 2015.* doi: 10.1126/sciadv.1601545

Copernicus Climate Change Service. (2018). *Climate Data Store.* Sea level gridded data from satellite observations for the global ocean from 1993 to present. Copernicus Climate Change Service (C3S) Climate Data Store (CDS). doi: 10.24381/cds.4c328c78

Desbruyères, D. G., Purkey, S. G., McDonagh, E. L., Johnson, G. C., & King, B. A. (2016). Deep and abyssal ocean warming from 35 years of repeat hydrography. *Geophysical Research Letters*, *43*(19), 356–10. doi: 10.1002/2016GL070413

Dieng, H. B., Palanisamy, H., Cazenave, A., Meyssignac, B., & von Schuckmann, K. (2015). *The Sea Level Budget Since 2003: Inference on the Deep Ocean Heat Content.* doi: 10.1007/s10712-015-9314-6

Ditlevsen, P., & Ditlevsen, S. (2023). Warning of a forthcoming collapse of the Atlantic meridional overturning circulation. *Nature Communications*, *14*(1), 4254. Retrieved from https://doi.org/10.1038/s41467-023-39810-w doi: 10.1038/s41467-023-39810-w

Domingues, C., Church, J., White, N., Gleckler, P., Wijffels, S., Barker, P., & Dunn, J. (2008). Improved estimates of upper-ocean warming and multi-decadal sea-level rise. *Nature*, *453*(7198), 1090–1093.

Feistel, R. (2012). TEOS-10: A new international oceanographic standard for seawater, ice, fluid water, and humid air. *International Journal of Thermophysics*, *33*. doi: 10.1007/s10765-010-0901-y

Frederikse, T., Landerer, F. W., Caron, L., Adhikari, S., Parkes, D., Humphrey, V. W., . . . Wu, Y. H. (2020). The causes of sea-level rise since 1900. *Nature*, *584*(7821), 393–397. Retrieved from http://dx.doi.org/10.1038/s41586-020-2591-3 doi: 10.1038/s41586-020-2591-3

Frederikse, T., Riva, R. E., & King, M. A. (2017). Ocean Bottom Deformation Due To Present-Day Mass Redistribution and Its Impact on Sea Level Observations. *Geophysical Research Letters*, *44*(24). doi: 10.1002/2017GL075419

Gill, A. E., & Niller, P. P. (1973). The theory of the seasonal variability in the ocean. *Deep-Sea Research and Oceanographic Abstracts*. doi: 10.1016/0011-7471(73)90049-1

Gould, J., Roemmich, D., Wuffels, S., Freeland, H., Ignaszewsky, M., Jianplng, X., . . . Riser, S. (2004). Argo profiling floats bring new era of in situ ocean observations. *Eos*, *85*. doi: 10.1029/2004eo190002

Gouretski, V., & Koltermann, K. P. (2004). WOCE global hydrographic climatology. *Berichte des BSH*, *35*, 1–52. doi: 10.5065/GS51-V170

Gunn, K. L., Rintoul, S. R., England, M. H., & Bowen, M. M. (2023). Recent reduced abyssal overturning and ventilation in the Australian Antarctic Basin. *Nature Climate Change*, *13*. doi: 10.1038/s41558-023-01667-8

Hansen, J., Sato, M., Kharecha, P., & Von Schuckmann, K. (2011). Earth's energy imbalance and implications. *Atmospheric Chemistry and Physics*. doi: 10.5194/acp-11-13421-2011

Harvey, T. C., Hamlington, B. D., Frederikse, T., Nerem, R. S., Piecuch, C. G., Hammond, W. C., . . . Boening, C. (2021). Ocean mass, sterodynamic effects, and vertical land motion largely explain US coast relative sea level rise. *Communications Earth and Environment*, *2*(233). doi: 10.1038/s43247-021-00300-w

Horwath, M., Gutknecht, B. D., Cazenave, A., Palanisamy, H. K., Marti, F., Marzeion, B., . . . Benveniste, J. (2022). *Global sea-level budget and ocean-mass budget, with a focus on advanced data products and uncertainty characterisation.* doi: 10.5194/essd-14-411-2022

Johnson, G. C. (2022). Antarctic Bottom Water Warming and Circulation Slowdown in the Argentine Basin From Analyses of Deep Argo and Historical

Shipboard Temperature Data. *Geophysical Research Letters*, *49*(18). doi: 10.1029/2022GL100526

Johnson, G. C., Cadot, C., Lyman, J. M., McTaggart, K. E., & Steffen, E. L. (2020). Antarctic Bottom Water Warming in the Brazil Basin: 1990s Through 2020, From WOCE to Deep Argo. *Geophysical Research Letters*, *47*(18). doi: 10.1029/2020GL089191

Johnson, G. C., & Lyman, J. M. (2020). Warming trends increasingly dominate global ocean. *Nature Climate Change*, *10*(8), 757–761. Retrieved from `http://dx.doi.org/10.1038/s41558-020-0822-0` doi: 10.1038/s41558-020-0822-0

Johnson, G. C., Lyman, J. M., & Purkey, S. G. (2015). Informing deep argo array design using argo and full-depth hydrographic section data. *Journal of Atmospheric and Oceanic Technology*, *32*. doi: 10.1175/JTECH-D-15-0139.1

Johnson, G. C., Purkey, S. G., Zilberman, N. V., & Roemmich, D. (2019). Deep Argo quantifies bottom water warming rates in the Southwest Pacific Basin. *Geophysical Research Letters*, *46*(5), 2662–2669. doi: 10.1029/2018GL081685

Kouketsu, S., Kawano, T., Masuda, S., Sugiura, N., Sasaki, Y., Toyoda, T., . . . others (2011). Deep ocean heat content changes estimated from observation and reanalysis product and their influence on sea level change. *J. Geophys. Res.*, *116*(C3).

Lele, R., Purkey, S. G., Nash, J. D., Mackinnon, J. A., Thurnherr, A. M., Whalen, C. B., . . . Talley, L. D. (2021). Abyssal Heat Budget in the Southwest Pacific Basin. *Journal of Physical Oceanography*, *51*(11), 3317–3333. doi: 10.1175/JPO-D-21-0045.1

Levitus, S., Antonov, J., & Boyer, T. (2005). Warming of the world ocean, 1955–2003. *Geophys. Res. Lett.*, *32*(2).

Levitus, S., Antonov, J. I., Boyer, T. P., Baranova, O. K., Garcia, H. E., Locarnini, R. A., . . . Zweng, M. M. (2012). World ocean heat content and thermosteric sea level change (0–2000 m), 1955–2010. *Geophys. Res. Lett.*, *39*(10). doi: 10.1029/2012GL051106

Levitus, S., Antonov, J. I., Boyer, T. P., & Stephens, C. (2000). Warming of the world ocean. *Science*. doi: 10.1126/science.287.5461.2225

Li, Q., England, M. H., Hogg, A. M. C., Rintoul, S. R., & Morrison, A. K. (2023). Abyssal ocean overturning slowdown and warming driven by Antarctic meltwater. *Nature*, *615*. doi: 10.1038/s41586-023-05762-w

Llovel, W., Balem, K., Tajouri, S., & Hochet, A. (2023). Cause of Substantial Global Mean Sea Level Rise Over 2014–2016. *Geophysical Research Letters*, *50*(19). doi: 10.1029/2023GL104709

Llovel, W., Purkey, S., Meyssignac, B., Blazquez, A., Kolodziejczyk, N., & Bamber, J. (2019). Global ocean freshening , ocean mass increase and global mean sea level rise over 2005 – 2015. *Scientific Reports*, 1–10. Retrieved from `http://dx.doi.org/10.1038/s41598-019-54239-2` doi: 10.1038/s41598-019-54239-2

Llovel, W., Willis, J. K., Landerer, F. W., & Fukumori, I. (2014). Deep-ocean contribution to sea level and energy budget not detectable over the past decade. *Nature Climate Change*, *4*. doi: 10.1038/nclimate2387

McDougall, P., Trevor J. ; Barker. (2011). Getting started with TEOS-10 and the Gibbs Seawater (GSW) Oceanographic Toolbox. *Scor/Iapso Wg127*.

Meyer et al. (2014). *Climate Change 2014*.

Moreira, L., Cazenave, A., Barnoud, A., & Chen, J. (2021). Sea-level fingerprints due to present-day water mass redistribution in observed sea-level data. *Remote Sensing*, *13*. doi: 10.3390/rs13224667

NASA/JPL. (2023). *JPL GRACE and GRACE-FO Mascon Ocean, Ice, and Hydrology Equivalent Water Height JPL Release 06.1 Version 03.* NASA Physical Oceanography Distributed Active Archive Center. Retrieved from `https://podaac.jpl.nasa.gov/dataset/TELLUS_GRAC-GRFO_MASCON_GRID_RL06.1_V3`

doi: 10.5067/TEMSC-3MJ63

Nerem, R. S., Beckley, B. D., Fasullo, J. T., Hamlington, B. D., Masters, D., & Mitchum, G. T. (2018). Climate-change–driven accelerated sea-level rise detected in the altimeter era. *Proceedings of the National Academy of Sciences of the United States of America*, *115*(9). doi: 10.1073/pnas.1717312115

Peltier, W. R., Argus, D. F., & Drummond, R. (2018). *Comment on "An Assessment of the ICE-6G_C (VM5a) Glacial Isostatic Adjustment Model" by Purcell et al.* doi: 10.1002/2016JB013844

Purkey, S. G., & Johnson, G. C. (2010a). Warming of Global Abyssal and Deep Southern Ocean Waters between the 1990s and 2000s: Contributions to Global Heat and Sea Level Rise Budgets. *J. Climate*, *23*, 6336–6351. doi: 10.1175/20

Purkey, S. G., & Johnson, G. C. (2010b). Warming of global abyssal and deep Southern Ocean waters between the 1990s and 2000s: Contributions to global heat and sea level rise budgets. *Journal of Climate*, *23*(23), 6336–6351. doi: 10.1175/2010JCLI3682.1

Purkey, S. G., & Johnson, G. C. (2012). Global Contraction of Antarctic Bottom Water between the 1980s and 2000s. *J. Climate*, *25*, 5830–5844.

Purkey, S. G., & Johnson, G. C. (2013). Antarctic Bottom Water warming and freshening: Contributions to sea level rise, ocean freshwater budgets, and global heat gain*. *Journal of Climate*. doi: 10.1175/JCLI-D-12-00834.1

Purkey, S. G., Johnson, G. C., & Chambers, D. P. (2014). Relative contributions of ocean mass and deep steric changes to sea level rise between 1993 and 2013. *Journal of Geophysical Research: Oceans*, *119*(11). doi: 10.1002/2014JC010180

Purkey, S. G., Johnson, G. C., Talley, L. D., Sloyan, B. M., Wijffels, S. E., Smethie, W., . . . Katsumata, K. (2019). Unabated Bottom Water Warming and Freshening in the South Pacific Ocean. *Journal of Geophysical Research: Oceans*, *124*(3), 1778–1794. doi: 10.1029/2018JC014775

Riser, S. C., Freeland, H. J., Roemmich, D., Wijffels, S., Troisi, A., Belbéoch, M., . . . Jayne, S. R. (2016). *Fifteen years of ocean observations with the global Argo array.* doi: 10.1038/nclimate2872

Roemmich, D., Alford, M. H., Claustre, H., Johnson, K. S., King, B., Moum, J., . . . Yasuda, I. (2019). On the future of Argo: A global, full-depth, multi-disciplinary array. *Frontiers in Marine Science*, *6*, 439. doi: 10.3389/fmars.2019.00439

Roemmich, D., & Gilson, J. (2009). The 2004-2008 mean and annual cycle of temperature, salinity, and steric height in the global ocean from the Argo Program. *Progress in Oceanography*, *82*. doi: 10.1016/j.pocean.2009.03.004

Roemmich, D., John Gould, W., & Gilson, J. (2012). 135 years of global ocean warming between the Challenger expedition and the Argo Programme. *Nature Climate Change*, *2*. doi: 10.1038/nclimate1461

Smeed, D. A., McCarthy, G. D., Cunningham, S. A., Frajka-Williams, E., Rayner, D., Johns, W. E., . . . Bryden, H. L. (2014). *Observed decline of the Atlantic meridional overturning circulation 2004-2012.* doi: 10.5194/os-10-29-2014

Stammer, D., & Cazenave, A. (2017). *Satellite altimetry over oceans and land surfaces.* doi: 10.1201/9781315151779

Steiner, A. K., Ladstädter, F., Randel, W. J., Maycock, A. C., Fu, Q., Claud, C., . . . Zou, C. Z. (2020). Observed temperature changes in the troposphere and stratosphere from 1979 to 2018. *Journal of Climate*. doi: 10.1175/JCLI-D-19-0998.1

Talley, L. D., Feely, R., Sloyan, B., Wanninkhof, R., Baringer, M., Bullister, J., . . . Zhang, J.-Z. (2016). Changes in Ocean Heat, Carbon Content, and Ventilation: A Review of the First Decade of GO-SHIP Global Repeat Hydrography. *Annual Review of Marine Science*. doi: 10.1146/annurev-marine-052915-100829

Talley, L. D., Sparrow, M., Chapman, P., & Gould, J. (2007). *Hydrographic Atlas of the World Ocean Circulation Experiment (WOCE). Volume 2: Pacific Ocean.*

Tapley, B. D., Bettadpur, S., Ries, J. C., Thompson, P. F., & Watkins, M. M. (2004). GRACE measurements of mass variability in the Earth system. *Science*. doi: 10.1126/science.1099192

Tapley, B. D., Watkins, M. M., Flechtner, F., Reigber, C., Bettadpur, S., Rodell, M., ... Velicogna, I. (2019). Contributions of GRACE to understanding climate change. *Nature Climate Change*, *9*(5), 358–369. Retrieved from `http://dx.doi.org/10.1038/s41558-019-0456-2` doi: 10.1038/s41558-019-0456-2

Tomczak, M., & Godfrey, J. S. (1994). Temperature, salinity, density and the oceanic pressure field. In *Regional oceanography.* doi: 10.1016/b978-0-08-041021-0.50006-0

Trenberth, K. E., Fasullo, J. T., & Balmaseda, M. A. (2014). Earth's energy imbalance. *Journal of Climate*, *27*. doi: 10.1175/JCLI-D-13-00294.1

Vishwakarma, B. D., Royston, S., Riva, R. E., Westaway, R. M., & Bamber, J. L. (2020). Sea Level Budgets Should Account for Ocean Bottom Deformation. *Geophysical Research Letters*, *47*(3). doi: 10.1029/2019GL086492

von Schuckmann, K., Minière, A., Gues, F., Cuesta-Valero, F. J., Kirchengast, G., Adusumilli, S., ... Zemp, M. (2022). *Heat stored in the Earth system 1960-2020: Where does the energy go?* World Data Center for Climate (WDCC) at DKRZ. Retrieved from `https://www.wdc-climate.de/ui/entry?acronym=GCOS_EHI_1960-2020`

Von Schuckmann, K., Palmer, M. D., Trenberth, K. E., Cazenave, A., Chambers, D. P., Champollion, N., ... Wild, M. (2016). *An imperative to monitor Earth's energy imbalance.* doi: 10.1038/nclimate2876

Watkins, M. M., Wiese, D. N., Yuan, D. N., Boening, C., & Landerer, F. W. (2015). Improved methods for observing Earth's time variable mass distribution with GRACE using spherical cap mascons. *Journal of Geophysical Research: Solid Earth.* doi: 10.1002/2014JB011547

Watson, C. S., White, N. J., Church, J., King, M. A., Burgette, R. J., & Legresy, B. (2015). Unabated global mean sea-level rise over the satellite altimeter era. *Nature Climate Change*, *5*. doi: 10.1038/nclimate2635

WCRP Global Sea Level Budget Group. (2018). Global sea-level budget 1993–present. *Earth System Science Data*, *10*(3), 1551–1590. Retrieved from `https://essd.copernicus.org/articles/10/1551/2018/` doi: 10.5194/essd-10-1551-2018

Wiese, D. N., Landerer, F. W., & Watkins, M. M. (2016). Quantifying and reducing leakage errors in the JPL RL05M GRACE mascon solution. *Water Resources Research*, *52*. doi: 10.1002/2016WR019344

Wong, A. P., Gilson, J., & Cabanes, C. (2023). Argo salinity: bias and uncertainty evaluation. *Earth System Science Data*, *15*(1). doi: 10.5194/essd-15-383-2023

Wunsch, C. (1996). *The Ocean Circulation Inverse Problem.* doi: 10.1017/cbo9780511629570